


## Hydrodynamic Effects on the Collapse Kinetics of Flexible Polyelectrolytes

Jiaying Yuan<sup>1</sup> and Hajime Tanaka<sup>1,2,\*</sup>

<sup>1</sup>*Research Center for Advanced Science and Technology, University of Tokyo,  
4-6-1 Komaba, Meguro-ku, Tokyo 153-8904, Japan*

<sup>2</sup>*Department of Fundamental Engineering, Institute of Industrial Science, University of Tokyo,  
4-6-1 Komaba, Meguro-ku, Tokyo 153-8505, Japan*

 (Received 5 July 2023; revised 5 November 2023; accepted 28 November 2023; published 18 January 2024)

Understanding the collapse kinetics of polyelectrolytes (PEs) is crucial for comprehending various biological and industrial phenomena. Despite occurring in an aqueous environment, previous computational studies have overlooked the influence of hydrodynamic interactions (HIs) facilitated by fluid motion. Here, we directly compute the Navier-Stokes equation to investigate the collapse kinetics of a highly charged flexible PE. Our findings reveal that HI accelerates PE collapse induced by hydrophobicity and multivalent salt. In the case of hydrophobicity, HI induces long-range collective motion of monomers, accelerating the coarsening of local clusters through either Brownian-coagulation-like or evaporation-condensation-like processes, depending on the strength of hydrophobicity with respect to electrostatic interaction. Regarding multivalent salt, HI does not affect the condensation dynamics of multivalent ions but facilitates quicker movement of local dipolar clusters along the PE, thereby expediting the collapse process. These results provide valuable insights into the underlying mechanisms of HI in PE collapse kinetics.

DOI: [10.1103/PhysRevLett.132.038101](https://doi.org/10.1103/PhysRevLett.132.038101)

Polyelectrolytes (PEs), polymers composed of charged repeating units, play critical roles in various industrial applications and biological processes [1–4]. They exhibit conformational responses when subjected to external stimuli, making them building blocks for designing smart materials [5–9]. It is worth noting that many biopolymers, such as proteins, DNA, and RNA, can be regarded as PEs. Therefore, understanding the collapse of PEs is crucial for unraveling the process of biomolecular folding [10–12] and chromatin compaction [3].

PEs have garnered considerable attention, resulting in extensive research on understanding their equilibrium structures [13–26]. However, the kinetic pathways of PE collapse have received comparatively less emphasis [27–31]. In a pioneering study on the collapse kinetics of PEs, the crucial roles of counterion valency, solvent quality, and counterion shape were systematically examined using Langevin simulations [28]. The work revealed the formation of intermediate pearl-necklace structures during PE collapse and showed a significant increase in the collapse rate as the counterion charge rose [28,30].

Nevertheless, previous studies have overlooked the influence of hydrodynamic interactions (HIs) mediated by fluid motion [32–37]. In neutral polymers, HIs play a dual role, expediting the collapse transition of a swollen polymer by inducing directional flow along the backbone [32,34,38] and retarding the collapse of a compact polymer, primarily due to the squeezing flow effect [34]. Considering the additional electrostatic interactions in PE,

the collapse behavior may exhibit even more diverse characteristics than polymers. However, despite the occurrence of PE collapse in an aqueous solution, the roles of HIs remain elusive.

In this Letter, we employ the fluid particle dynamics (FPD) method [39–41] with fully resolved electrostatics and HIs to investigate the collapse kinetics of a representative PE [14,16] induced by hydrophobicity and multivalent salt. We find the significant role of HI in accelerating the collapse under both conditions. Specifically, for hydrophobicity-induced collapse, HI enhances the coarsening of pearl-like clusters through either a Brownian-coagulation-like or evaporation-condensation-like mechanism, depending on hydrophobicity strength. During multivalent salt-induced collapse, HI has minimal impact on the condensation dynamics of multivalent ions initially but accelerates the motion of local dipolar clusters, expediting collapse.

Our coarse-grained (CG) model comprises an anionic PE and monovalent counterions with a charge of  $q = e$  in a cubic three-dimensional periodic box of size  $L$ . The PE is represented as a bead-spring chain [13,14,16,18,42] consisting of  $N_{\text{pol}} = 96$  monomers, each typically carrying a charge of  $-q$ . The system is devoid of salt in the investigation of hydrophobicity-induced collapse. However, in salt-induced collapse, an additional salt with a concentration of  $c_s$  is introduced, dissociating into cations with a charge of  $Zq$  and monovalent anions. Both the monomers and ions are modeled as spheres with a diameter of  $\sigma$ , interacting via a Lennard-Jones (LJ) potential with a coupling constant of  $\epsilon$

and a cutoff distance of  $r_{\text{cut}}$ . The Bjerrum length is given by  $l_B = e^2/(4\pi k_B T \epsilon_{\text{sol}}) = 0.72$  nm, where  $\epsilon_{\text{sol}}$  is the permittivity of the solvent,  $k_B$  is Boltzmann's constant, and  $T$  is the absolute temperature. Following the convention [14,16] for aqueous PE simulations, we adopt  $\sigma = l_B$  to represent a typical size of hydrated ions and ionizable groups. Electrostatic interactions are computed using the Ewald summation [43,44]. To incorporate HI, we utilize the FPD method [39–41], solving the Navier-Stokes (NS) equation directly [45]. For comparisons, we conduct Brownian dynamics (BD) simulations. As the time unit, we employ the Brownian time for a free particle,  $\tau_{\text{BD}}$ . Further details, model limitations [46–48], and computational cost are provided in the Supplemental Material [49].

Now, we investigate the PE collapse induced by hydrophobicity in a salt-free solution. The dependence of the equilibrium squared radius of gyration,  $R_g^2$  (see Ref. [49] for the definition), on the strength of hydrophobic attraction,  $\epsilon/k_B T$ , along with free-energy profiles [52] are depicted in Fig. S2 in [49]. Figure 1(a) shows the temporal evolution of  $R_g^2$  for a PE chain induced by the solvent quality change from a good solvent to a poor solvent of  $\epsilon/k_B T = 5$ . It is evident that HI expedites the collapse process compared to BD simulations [Fig. 1(a)]. Figure 1(c) (also Movie S1) provides representative snapshots of the PE configurations during collapsing in FPD simulations. We can see that local clusters initially form and

subsequently undergo a coarsening process [Fig. 1(c)], a scenario also observed in the collapse of a neutral polymer [32,34,53]. The temporal evolution of the cluster number,  $N_c$  (see Ref. [49] for definition), illustrates that HI accelerates the coarsening [Fig. 1(d)]. We attribute this accelerated monomer aggregation to the flow surrounding the PE, which induces long-range cooperative movements surpassing the behavior observed in free-draining BD simulations without HI. This long-range cooperative movement, identified by the extended spatial correlation of particle velocity (Fig. 4), originates from the HI: A polymer bead in motion generates a flow that influences nearby beads, causing them to move in alignment with its trajectory. This influence overcomes the electrostatic repulsion that would otherwise impede the coarsening process.

The growth of monomer numbers within each cluster [Fig. 1(e) for FPD and Fig. S3(a) in [49] for BD] follows a stepwise pattern, resembling the coarsening mechanism observed in the Brownian-coagulation scenario for droplet-like phase separation of attractive uncharged monomers characterized by a power law  $\langle q \rangle \sim t^{-1/3}$  and  $\langle R \rangle \sim t^{1/3}$ , where  $\langle q \rangle$  is the characteristic wave number (see Ref. [49] for definition) and  $\langle R \rangle = 2\pi/\langle q \rangle$  is the characteristic size of droplet-like clusters [54–56]. We indeed observe  $\langle q \rangle \sim t^{-1/3}$  [Fig. 1(b)],  $\langle R \rangle \sim t^{1/3}$  [the inset of Fig. 1(b)], and  $n_{\text{max}} \sim (\langle R \rangle/\sigma)^3 \sim t$  [Fig. 1(f)] where  $n_{\text{max}}$  denotes the characteristic particle number within the largest cluster.

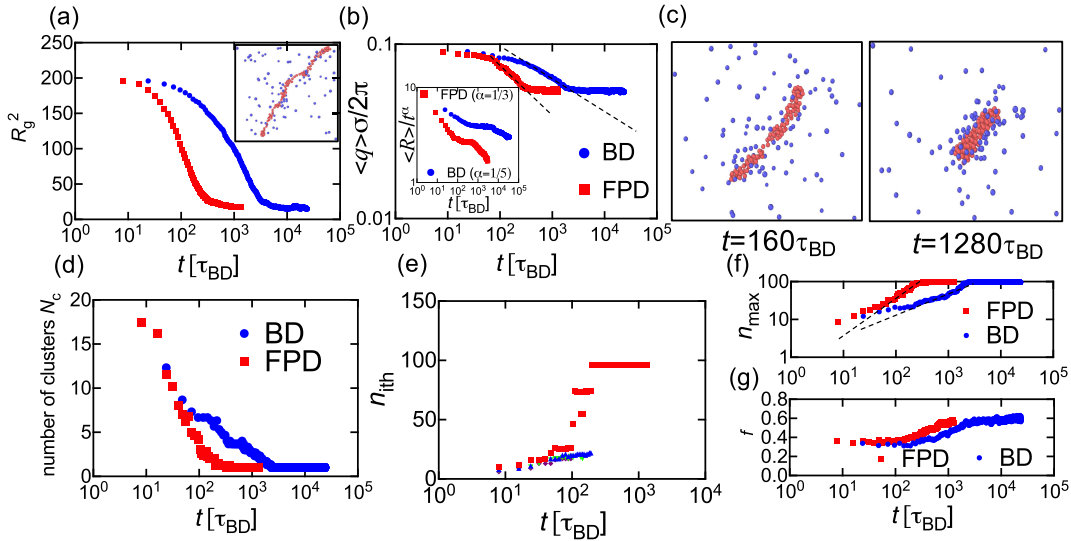


FIG. 1. Hydrophobicity-driven collapse of a polyelectrolyte from a good solvent condition to  $\epsilon/k_B T = 5$ . (a) Evolution of squared radius of gyration,  $R_g^2$ , over time in BD (blue line) and FPD (red line) simulations. The inset shows the initial condition of an expanded PE (red beads: PE monomers; blue beads: counterions). (b) Temporal change of the characteristic wave number,  $\langle q \rangle$ , with the dashed lines indicating slopes of  $-1/3$  and  $-1/5$ . The inset shows  $\langle R \rangle/t^\alpha$ , where  $\langle R \rangle = 2\pi/\langle q \rangle$  represents the characteristic size of individual clusters ( $\alpha = 1/3$  for FPD and  $\alpha = 1/5$  for BD). Notably,  $\langle R \rangle/t^\alpha$  remains constant across a specific range, providing evidence of power-law coarsening. (c) Snapshots from FPD simulations depicting the temporal change of PE conformation during the collapse process. (d) Temporal change in the number of clusters,  $N_c$ . (e) The number of monomers in the top four largest clusters. Cluster sizes are sorted by the number of constituent monomers, with larger clusters taking precedence. See Ref. [49] for the cluster definition. (f) Temporal change of the number of monomers in the largest cluster,  $n_{\text{max}}$ , with dashed lines indicating slopes of 1 and  $3/5$ . (g) Temporal change of the fraction of condensed counterions (within a cutoff distance  $2.5\sigma$  around the PE).

Notably, power-law coarsening has also been reported for the collapse of a neutral polymer [53], suggesting a more dominant role for hydrophobic attraction. We compare the structure factor  $S(q, t)$  (see Ref. [49] for definition) with the analytical results of neutral polymer collapse [53] (Fig. S4 in [49]), supporting the notion that the coarsening kinetics during the collapse of PEs under poor solvent conditions closely resemble those of neutral polymers. Nevertheless, in the later stages of this collapse, the globule maintains a cylindrical shape with an asphericity degree of approximately  $A \approx 0.6$  [Fig. 1(c)]. The persistence of this cylindrical structure can be attributed to electrostatic repulsion, creating a substantial energy barrier that hinders the transition from a cylindrical configuration to a more compact form. While this transition occurs rapidly during the collapse of neutral polymers, the presence of electrostatic forces significantly slows it down, preventing direct observation of such a shape change within our simulations.

On the contrary,  $\langle q \rangle \sim t^{-1/5}$  is found in BD [Fig. 1(b)]. We also find  $\langle q \rangle \sim t^{-1/5}$  in BD simulations of Brownian-coagulation coarsening of uncharged monomers (data not shown). This indicates the fundamental failure of BD in properly modeling the coarsening dynamics and further supports the essential roles of HI. The physical mechanism behind the exponent of  $1/5$  is out of the scope of this Letter, and thus, we will discuss this topic elsewhere, in connection to phase separation dynamics. Additionally, during the collapse of the PE, we observe an accumulation of monovalent counterions onto the chain, and HI accelerates this condensation process [Fig. 1(g)].

The power-law coarsening  $\langle q \rangle \sim t^{-1/3}$  is also evident under  $\varepsilon/k_B T = 4$  [Fig. 5(a)]. However, it is worth

noting that, generally,  $\varepsilon/k_B T > 3$  is unlikely for PEs, as charged monomers typically exhibit weaker hydrophobicity. Nevertheless, such a situation may be relevant for hydrophobic-grafted PEs [57]. Another practically important case involves PEs with a mix of charged and uncharged monomers, where the charge fraction is denoted as  $\phi$ . Considering that electrostatic repulsion acts only between a pair of charged monomers, its effective contact energy is reduced to  $l_B k_B T \phi^2 / \sigma$ . Thus, the relative dominance of hydrophobicity (energy scale  $\varepsilon$ ) over electrostatics is characterized by a dimensionless parameter  $\Gamma \sim \varepsilon \sigma / (\phi^2 l_B k_B T)$ , which is  $\Gamma \sim (\varepsilon / k_B T) \phi^{-2}$  in our setting  $l_B = \sigma$ . Interestingly, we observe power-law coarsening for the collapse of PE under conditions  $(\varepsilon/k_B T, \phi) = (3, 0.75)$  [Fig. 5(c)],  $(\varepsilon/k_B T, \phi) = (2.6, 0.75)$  [Fig. 5(d)],  $(\varepsilon/k_B T, \phi) = (2.1, 0.67)$  [Fig. 5(f)],  $(\varepsilon/k_B T, \phi) = (2.9, 0.8)$  [Fig. 5(h)], and  $(\varepsilon/k_B T, \phi) = (1.7, 0.6)$  [Fig. S5(a) in [49]]. These results indicate when  $\Gamma \gtrsim 4$ , PE collapse exhibits  $\langle q \rangle \sim t^{-1/3}$  with HI whereas  $\langle q \rangle \sim t^{-1/5}$  without HI. This mirrors the collapse of neutral polymers driven solely by hydrophobic interaction.

We proceed with the investigation of PE collapse kinetics under a weaker hydrophobic attraction strength of  $\varepsilon/k_B T = 3$ . The results are summarized in Fig. 2. Similar to the  $\varepsilon/k_B T = 5$  case, the inclusion of HI significantly accelerates the collapse of the PE [Fig. 2(a); also see the inset of Fig. 2(a) for  $\langle q \rangle$ ]. Under this condition, the interplay between electrostatic repulsion, favoring chain expansion, and hydrophobic attraction, stabilizing the collapsed chain, leads to the formation of equilibrium pearl-necklace structures consisting of approximately three to four pearls [Fig. 2(c); also see Fig. 2(b) and Movie S2].

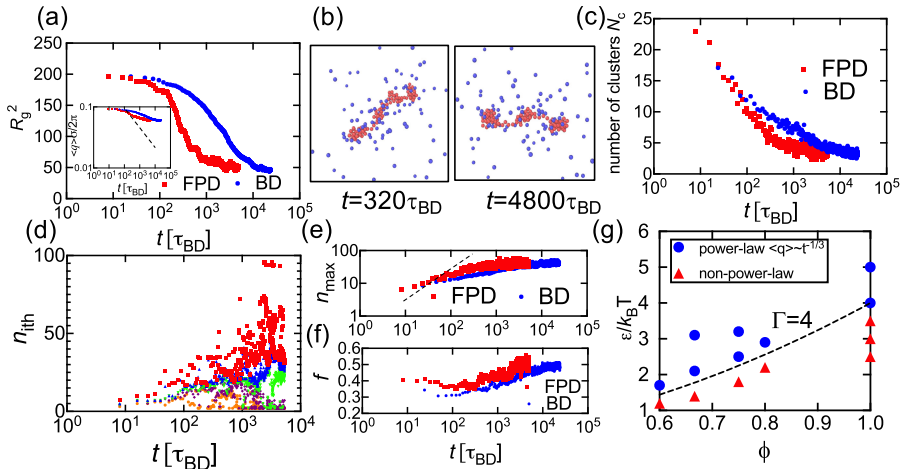


FIG. 2. Hydrophobicity-driven polyelectrolyte collapse in response to a solvent quality change from a good solvent to a poor solvent with  $\varepsilon/k_B T = 3$ . The analyses presented in panels (a)–(f) correspond to those in Fig. 1. In both cases, the presence of HI accelerates the collapse, albeit through different coarsening mechanisms (see the text for details). The dashed lines in the inset of (a) and (e) exhibit slopes of  $-1/3$  and  $1$ , respectively. (g) State diagram as a function of  $\varepsilon/k_B T$  and charge fraction  $\phi$ . The circles and triangles correspond to the coarsening with and without the power-law behavior  $\langle q \rangle \sim t^{-1/3}$ . The dashed line represents  $\Gamma = \varepsilon \sigma / (\phi^2 l_B k_B T) = 4$ , serving as a boundary.

These pearl-necklace structures have been previously reported in simulations [24,28] and observed experimentally [58].

In contrast to Fig. 1(e), the growth of cluster sizes, in this case, exhibits the characteristic features of an evaporation-condensation scenario [59,60], where larger clusters [e.g., red, blue, and green lines in Fig. 2(d)] grow at the expense of absorbing monomers from smaller clusters [e.g., purple and orange lines in Fig. 2(d)]. The exchange of monomers primarily occurs within the stringlike regions connecting neighboring clusters. The same coarsening mechanism is also observed in BD simulations [Fig. S3(b) in [49]]. However, the temporal evolution of  $n_{\max}$  [Fig. 2(e)] and  $\langle q \rangle$  [the inset of Fig. 2(a)] is much slower than  $n_{\max} \sim t$  and  $\langle q \rangle \sim t^{-1/3}$  of evaporation-condensation coarsening of uncharged monomers [59,60], which is due to significant electrostatic repulsion that frustrates the coarsening. Furthermore, the enhanced condensation of monovalent counterions upon PE collapse is observed [Fig. 2(f)], although the final equilibrium value  $f_{\text{eq}} \sim 50\%$  is smaller compared to  $f_{\text{eq}} \sim 60\%$  observed under  $\varepsilon/k_B T = 5$  [Fig. 1(g)]. This difference can be attributed to the lesser degree of collapse exhibited by the PE under weaker hydrophobic attraction.

The effects of HI on accelerating collapse mentioned above hold generally for  $\varepsilon/k_B T = 2.5$  (Fig. 6). Notably, the presence of HI even leads to an over-collapsing phenomenon followed by subsequent reexpansion. This behavior can be attributed to a combination of relatively flat free-energy profiles around the equilibrium value of  $R_g$  [Fig. S2(b) in [49]] and transient excessive condensation of counterions that results in stronger screenings of electrostatic repulsion [Fig. 6(b)]. The excessive condensation is primarily caused by the flow fields generated by PE collapse, underscoring a significant influence of fluid momentum.

The absence of power-law coarsening  $\langle q \rangle \sim t^{-1/3}$  is also observed for  $(\varepsilon/k_B T, \phi) = (3.5, 1)$  [Fig. 5(b)],  $(\varepsilon/k_B T, \phi) = (1.8, 0.75)$  [Fig. 5(e)],  $(\varepsilon/k_B T, \phi) = (1.4, 0.67)$  [Fig. 5(g)],  $(\varepsilon/k_B T, \phi) = (2.2, 0.8)$  [Fig. 5(i)], and  $(\varepsilon/k_B T, \phi) = (1.2, 0.6)$  [Fig. S5(b) in [49]], highlighting the critical role of electrostatics for  $\Gamma < 4$ . We present a state diagram [Fig. 2(g)] that categorizes the coarsening into cases with and without  $\langle q \rangle \sim t^{-1/3}$ . It is noteworthy that  $\Gamma = 4$  properly represents the border. Importantly, HI expedites the collapse of PE across the entire parameter range we have examined, which is relevant for practical applications. Moreover, by varying the chain length,  $N_{\text{pol}}$ , we verify that the impact of HI on accelerating collapse is amplified for longer chains (Fig. 7). Thus, the effect of HI should be highly relevant to a realistic (long) PE. Additional discussions on the difference in the collapse time between a PE and neutral polymer are provided in Appendix A, and the possible connection of our findings to biopolymers is explored in Appendix B.

In addition to hydrophobicity, the collapse of PEs triggered by multivalent salt is also a common phenomenon in nature and biology [4]. Thus, we further investigate the kinetics of PE collapse induced by multivalent ( $Z:1$ ) salt (see Fig. S6 in [49] for equilibrium conformations), specifically at a salt concentration  $c_s \approx c_m/Z$ , where  $c_m = N_{\text{pol}}/L^3 \approx 0.0023\sigma^{-3}$  represents the monomer concentration. Previous simulations have shown that PE collapse is most pronounced when  $c_s \approx c_m/Z$  [20].

Similar to hydrophobicity-induced collapse, the presence of HI accelerates the collapse induced by multivalent salt [Fig. 3(a)]. However, the temporal change in the fraction of condensed multivalent ions is nearly the same between BD and FPD simulations [Fig. 3(b), top]. This indicates that HI has little influence on the ion condensation dynamics, primarily governed by the diffusion of multivalent ions. Analysis of the size of the largest clusters reveals that there is no coarsening of local clusters [Fig. 3(b), bottom]. This behavior qualitatively differs from the hydrophobicity-induced PE collapse, where coarsening of local clusters is observed. Additionally, we observed that the size of local clusters is similar between BD and

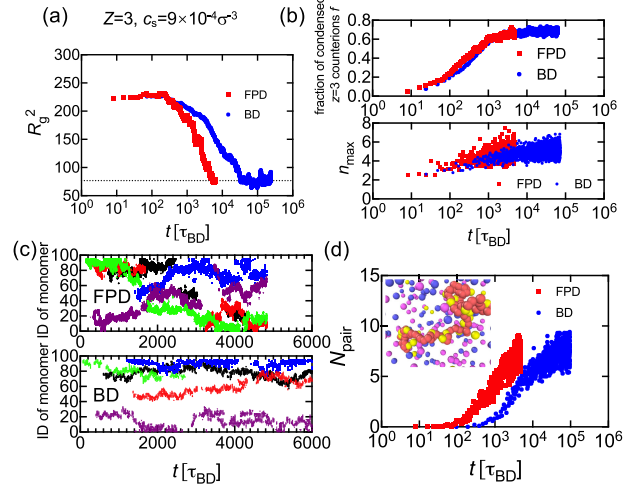


FIG. 3. Trivalent salt-induced polyelectrolyte collapse. (a) Temporal change of the squared radius of gyration,  $R_g^2$ , of a PE in the presence of trivalent salt (salt concentration  $c_s = 0.0009\sigma^{-3}$ ) in BD (blue line) and FPD (red line) simulations. (b) Top: Temporal change of the fraction of condensed trivalent counterions. Bottom: Temporal change in the number of monomers in the largest cluster,  $n_{\max}$ . (c) Temporal change of the monomer ID (1–96) to which a trivalent counterion is bound, depicted separately for FPD (top) and BD (bottom) simulations. Five representative counterions are illustrated; the other counterions show qualitatively similar behaviors. (d) Temporal change of the number of condensed cation-cation pairs,  $N_{\text{pair}}$ , in BD (blue line) and FPD (red line) simulations. The inset shows the equilibrium conformation of a collapsed PE (red beads: PE monomers; blue beads: counterions; yellow beads: trivalent cations; magenta beads: monovalent anions).



FPD simulations. These results support that the slow collapse observed in BD is not attributable to differences in the condensation of multivalent cations or the formation of local clusters.

The PE collapse due to multivalent ions is primarily driven by weak attractions between dipoles formed by multivalent cations and the negatively charged monomers bound to them after the condensation of multivalent cations (see also Movie S3 for divalent salt and Movie S4 for trivalent salt). Such attractive dipolar intrachain interactions have been known to be responsible for the collapse of a free PE [61]. In the presence of HI, these dipole-dipole attractions induce the motion of the PE, resulting in complex flow fields. This flow can enhance the transport of condensed cations (i.e., dipoles) along the chains, leading to the formation of dipolar pairs. Consequently, HI accelerates the collapse. In the absence of HI, the formation of dipolar pairs is governed by thermal diffusion alone, resulting in slower collapse.

This scenario is supported by the observation of the dynamic motion of condensed multivalent ions along the polymer chain. The condensed multivalent ions exhibit motion along the chain rather than remaining static, primarily due to the electrostatic attraction between a multivalent cation and the nearest monomer, which is on the order of  $2 \sim 3k_B T$  [Fig. 3(c)]. Notably, the presence of HI accelerates the motion of multivalent cations [Fig. 3(c), top], whereas, in BD simulations, they exhibit localized motion for an extended period [Fig. 3(c), bottom]. The faster motion of multivalent cations accelerates the ion pair formation of dipolar clusters [Fig. 3(d)], which is responsible for the significantly faster collapse observed in the presence of HI. The roles of HI in PE collapse induced by divalent salt ( $c_s = 0.0012\sigma^{-3}$ ; Fig. S7 in [49]) are qualitatively similar.

In summary, we have utilized the FPD method [39–41] to elucidate the impact of HI on the kinetics of the collapse of a highly charged PE induced by hydrophobicity and multivalent salt. Our study highlights the crucial role of HI in accelerating the collapse. In the case of hydrophobicity-driven collapse, HI facilitates longer-range collective motion of monomers and accelerates the coarsening of pearl-like clusters. These processes proceed through mechanisms reminiscent of Brownian coagulation and evaporation and condensation mechanisms, respectively, for cases characterized by strong and weak hydrophobicity relative to electrostatic interactions. Specifically, in the former, the coarsening kinetics follows a power-law behavior with  $\langle q \rangle \sim t^{-1/3}$  in the presence of HI, in contrast to  $\langle q \rangle \sim t^{-1/5}$  when HI is ignored. Regarding multivalent salt-induced collapse, HI has a marginal effect on the condensation dynamics of multivalent ions. However, it facilitates faster motion of local dipolar clusters along the

PE chain, thereby enhancing chain relaxation and accelerating the collapse process. Our findings offer potential applications in designing smart materials that require precise control over PE collapse dynamics [62]. Moreover, our approach can be extended to hydrodynamic modeling of more complex PE systems [4].

We are grateful to the anonymous referees for their comments, which have contributed to the improvement of the manuscript. This work was partially supported by the Grant-in-Aid for Specially Promoted Research (JSPS KAKENHI Grant No. JP20H05619) from the Japan Society for the Promotion of Science (JSPS). The authors acknowledge the Information Technology Center at The University of Tokyo. J. Y. is grateful to Tine Curk and Yanwei Wang for discussions on polyelectrolyte collapse.

*Appendix A: Collapse timescales of a polyelectrolyte and a neutral polymer.*—Generally, the collapse of a polyelectrolyte (PE) exhibits a notable deceleration compared to a neutral polymer due to electrostatic repulsion, which persists regardless of the presence or absence of HI (Fig. S8 in [49]). However, the deceleration is more pronounced in BD. For example, under  $\varepsilon/k_B T = 2 \sim 3$ , the collapsing time of PEs is extended nearly tenfold in BD compared to uncharged polymers (compare the BD data of Fig. 2(a) and Figs. S8(a)–(b) in [49]). Conversely, when HI is introduced, the retardation is partially canceled, causing the collapsing time to increase by approximately four- to fivefold. Thus, the influence of HI on the collapsing kinetics is more critical for a PE.

*Appendix B: Connection to biopolymer collapse.*—Our findings illuminate the potential to utilize HI for achieving

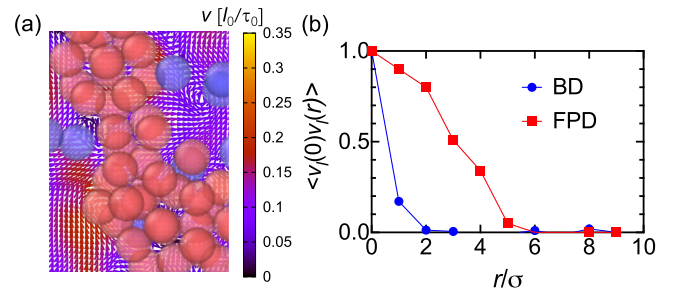


FIG. 4. Characterization of flow field during the collapse of a polyelectrolyte. (a) Flow velocity field  $v$  (unit  $l_0/\tau_0$ ;  $l_0$  is the length unit, and  $\tau_0$  is the time unit in FPD; see Ref. [49] for details) surrounding a PE undergoing collapse from a good solvent to  $\varepsilon/k_B T = 5$ . (b) Spatial correlation function of the monomer velocity  $v_i(0) \cdot v_i(r)$  along the long axis for the PE in (a). We can see that the presence of HI induces longer-ranged cooperative motion of monomers compared to free-draining BD simulations.

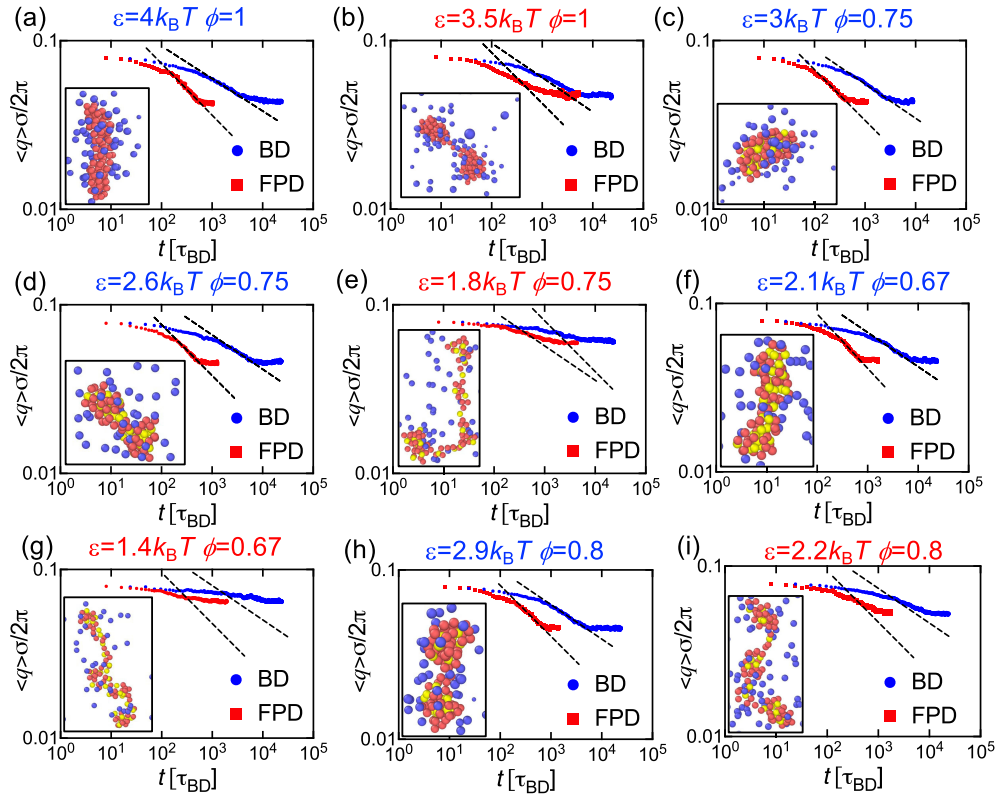


FIG. 5. Temporal evolution of the characteristic wave number  $\langle q \rangle$  in BD (blue line) and FPD (red line) simulations for PE collapse induced by a solvent quality change from a good solvent to a poor solvent where (a) strength of hydrophobic attraction  $\epsilon/k_B T = 4$  and charge fraction  $\phi = 1$ , (b)  $\epsilon/k_B T = 3.5$  and  $\phi = 1$ , (c)  $\epsilon/k_B T = 3$  and  $\phi = 0.75$ , (d)  $\epsilon/k_B T = 2.6$  and  $\phi = 0.75$ , (e)  $\epsilon/k_B T = 1.8$  and  $\phi = 0.75$ , (f)  $\epsilon/k_B T = 2.1$  and  $\phi = 0.67$ , (g)  $\epsilon/k_B T = 1.4$  and  $\phi = 0.67$ , (h)  $\epsilon/k_B T = 2.9$  and  $\phi = 0.8$ , and (i)  $\epsilon/k_B T = 2.2$  and  $\phi = 0.8$ . Insets in each panel show the final PE conformation in FPD simulations (yellow-colored beads: neutral monomers; red-colored beads: negatively charged monovalent monomers; blue-colored beads: counterions). Dashed lines represent slopes of  $-1/3$  and  $-1/5$ .

more rapid collapsing of biopolymers. For example, we observe HI expedites the collapse of a charged polymer chain composed of two-thirds uncharged hydrophobic

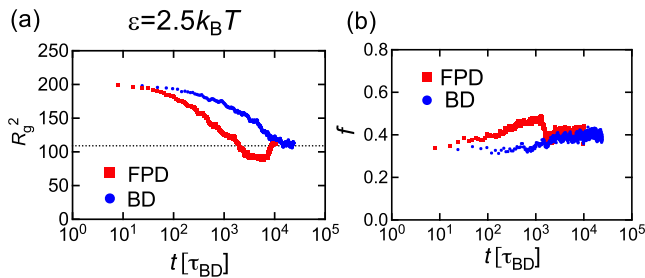


FIG. 6. Temporal change of (a) the squared radius of gyration,  $R_g^2$ , and (b) the condensed counterion fraction in BD (blue line) and FPD (red line) simulations for a PE collapse induced by a solvent quality change from a good solvent to a poor solvent with  $\epsilon/k_B T = 2.5$ .

monomers (hydrophobic attraction  $\epsilon/k_B T = 1.8$ ) and one-third charged hydrophilic monomers, which can be a primitive model of a peptide chain (Fig. S9 in [49]). Additionally, we observe the power-law coarsening behavior of  $\langle q \rangle \sim t^{-1/3}$  (Fig. S9 in [49]), suggesting that hydrophobic attraction is the dominant factor driving the collapse kinetics in this case. We expect that by examining the time evolution of  $\langle q \rangle$ , we may also infer which of the hydrophobic and electrostatic interactions plays a more dominant role in the collapse dynamics of biopolymers: The former should exhibit power-law coarsening of  $\langle q \rangle \sim t^{-1/3}$  with HI, whereas the latter should not. We hope our results will encourage researchers to verify our predictions in *in vitro* experiments where HI and electrostatics are not screened, enhancing our fundamental understanding of the complex interplay among hydrodynamics, electrostatics, and hydrophobic interactions in the collapsing and folding of biopolymers [63–65].

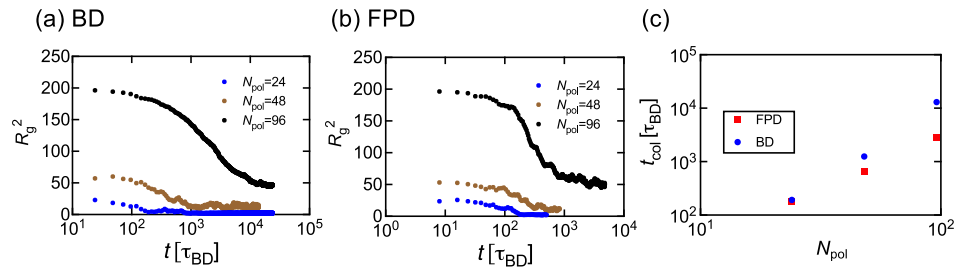


FIG. 7. Temporal change of the squared radius of gyration,  $R_g^2$ , in (a) BD and (b) FPD simulations for the collapse of a PE with varying chain length  $N_{pol} = 24 \sim 96$  induced by a solvent quality change from a good solvent to a poor solvent with  $\epsilon/k_B T = 3$ . (c) Collapse timescale dependence on the chain length,  $N_{pol}$ , in BD (blue circles) and FPD (red squares) simulations.

\*tanaka@iis.u-tokyo.ac.jp

- [1] Fumio Oosawa, *Polyelectrolytes* (Marcel Dekker, New York, 1971).
- [2] *Handbook of Polyelectrolytes and Their Applications*, edited by Sukant K. Tripathy, Jayant Kumar, and Hari Singh Nalwa (American Scientific, Valencia, 2002), Vol. I, II, III.
- [3] Michael Rubinstein and Gargin A Papoian, Polyelectrolytes in biology and soft matter, *Soft Matter* **8**, 9265 (2012).
- [4] Murugappan Muthukumar, *Physics of Charged Macromolecules: Synthetic and Biological Systems* (Cambridge University Press, Cambridge, England, 2022).
- [5] Martien A. Cohen Stuart, Wilhelm T. S. Huck, Jan Genzer, Marcus Müller, Christopher Ober, Manfred Stamm, Gleb B. Sukhorukov, Igal Szleifer, Vladimir V. Tsukruk, Marek Urban, Françoise Winnik, Stefan Zauscher, Igor Luzinov, and Sergiy Minko, Emerging applications of stimuli-responsive polymer materials, *Nat. Mater.* **9**, 101 (2010).
- [6] Shashishekar P. Adiga and Donald W. Brenner, Stimuli-responsive polymer brushes for flow control through nanopores, *J. Funct. Biomater.* **3**, 239 (2012).
- [7] Guang Chen and Siddhartha Das, Electroosmotic transport in polyelectrolyte-grafted nanochannels with pH-dependent charge density, *J. Appl. Phys.* **117**, 185304 (2015).
- [8] Mario Tagliacuzzi and Igal Szleifer, Transport mechanisms in nanopores and nanochannels: Can we mimic nature?, *Mater. Today* **18**, 131 (2015).
- [9] Jiaxing Yuan, Hanne S. Antila, and Erik Lijten, Dielectric effects on ion transport in polyelectrolyte brushes, *ACS Macro Lett.* **8**, 183 (2019).
- [10] V. A. Bloomfield, Condensation of DNA by multivalent cations: Considerations on mechanism, *Biopolymers* **31**, 1471 (1991).
- [11] Rick Russell, Ian S. Millett, Mark W. Tate, Lisa W. Kwok, Bradley Nakatani, Sol M. Gruner, Simon G. J. Mochrie, Vijay Pande, Sebastian Doniach, Daniel Herschlag *et al.*, Rapid compaction during RNA folding, *Proc. Natl. Acad. Sci. U.S.A.* **99**, 4266 (2002).
- [12] Sonja Müller-Späh, Andrea Soranno, Verena Hirschfeld, Hagen Hofmann, Stefan Rügger, Luc Reymond, Daniel Nettels, and Benjamin Schuler, Charge interactions can dominate the dimensions of intrinsically disordered proteins, *Proc. Natl. Acad. Sci. U.S.A.* **107**, 14609 (2010).
- [13] M. J. Stevens and K. Kremer, Structure of salt-free linear polyelectrolytes, *Phys. Rev. Lett.* **71**, 2228 (1993).
- [14] Mark J. Stevens and Kurt Kremer, The nature of flexible linear polyelectrolytes in salt free solution: A molecular dynamics study, *J. Chem. Phys.* **103**, 1669 (1995).
- [15] Andrey V. Dobrynin, Michael Rubinstein, and Sergei P. Obukhov, Cascade of transitions of polyelectrolytes in poor solvents, *Macromolecules* **29**, 2974 (1996).
- [16] M. J. Stevens and S. J. Plimpton, The effect of added salt on polyelectrolyte structure, *Eur. Phys. J. B* **2**, 341 (1998).
- [17] P. Chodanowski and S. Stoll, Monte Carlo simulations of hydrophobic polyelectrolytes: Evidence of complex configurational transitions, *J. Chem. Phys.* **111**, 6069 (1999).
- [18] U. Micka, C. Holm, and K. Kremer, Strongly charged, flexible polyelectrolytes in poor solvents: Molecular dynamics simulations, *Langmuir* **15**, 4033 (1999).
- [19] F. J. Solis and M. Olvera de la Cruz, Collapse of flexible polyelectrolytes in multivalent salt solutions, *J. Chem. Phys.* **112**, 2030 (2000).
- [20] Pai-Yi Hsiao and Erik Lijten, Salt-induced collapse and reexpansion of highly charged flexible polyelectrolytes, *Phys. Rev. Lett.* **97**, 148301 (2006).
- [21] Chwen-Yang Shew and Arun Yethiraj, Conformational properties of isolated polyelectrolytes in poor solvents, *J. Chem. Phys.* **110**, 676 (1999).
- [22] Bahattin M. Baysal and Frank E. Karasz, Coil-globule collapse in flexible macromolecules, *Macromol. Theory Simul.* **12**, 627 (2003).
- [23] Rakwoo Chang and Arun Yethiraj, Strongly charged flexible polyelectrolytes in poor solvents: Molecular dynamics simulations with explicit solvent, *J. Chem. Phys.* **118**, 6634 (2003).

- [24] H. J. Limbach and C. Holm, Single-chain properties of polyelectrolytes in poor solvent, *J. Phys. Chem. B* **107**, 8041 (2003).
- [25] Anoop Varghese, Satyavani Vemparala, and R Rajesh, Phase transitions of a single polyelectrolyte in a poor solvent with explicit counterions, *J. Chem. Phys.* **135**, 154902 (2011).
- [26] Chao Duan, Weihua Li, and Rui Wang, Conformation of a single polyelectrolyte in poor solvents, *J. Chem. Phys.* **153**, 064901 (2020).
- [27] Namkyung Lee and D. Thirumalai, Dynamics of collapse of flexible polyampholytes, *J. Chem. Phys.* **113**, 5126 (2000).
- [28] Namkyung Lee and D Thirumalai, Dynamics of collapse of flexible polyelectrolytes in poor solvents, *Macromolecules* **34**, 3446 (2001).
- [29] N-K Lee and S Obukhov, Collapse dynamics of a polyelectrolyte, *Europhys. Lett.* **66**, 350 (2004).
- [30] Ngo Minh Toan, Bae-Yeun Ha, and Dave Thirumalai, Polyelectrolyte and polyampholyte effects in synthetic and biological macromolecules, in ionic interactions in *Natural and Synthetic Macromolecules* (John Wiley, New York, 2012), Chap. 4, pp. 91–119.
- [31] Susmita Ghosh and Satyavani Vemparala, Kinetics of charged polymer collapse in poor solvents, *J. Phys. Condens. Matter* **34**, 045101 (2021).
- [32] N. Kikuchi, A. Gent, and J. M. Yeomans, Polymer collapse in the presence of hydrodynamic interactions, *Eur. Phys. J. E* **9**, 63 (2002).
- [33] Hajime Tanaka, Roles of hydrodynamic interactions in structure formation of soft matter: Protein folding as an example, *J. Phys. Condens. Matter* **17**, S2795 (2005).
- [34] Kumiko Kamata, Takeaki Araki, and Hajime Tanaka, Hydrodynamic selection of the kinetic pathway of a polymer coil-globule transition, *Phys. Rev. Lett.* **102**, 108303 (2009).
- [35] Akira Furukawa and Hajime Tanaka, Key role of hydrodynamic interactions in colloidal gelation, *Phys. Rev. Lett.* **104**, 245702 (2010).
- [36] Michio Tateno and Hajime Tanaka, Power-law coarsening in network-forming phase separation governed by mechanical relaxation, *Nat. Commun.* **12**, 912 (2021).
- [37] Jiaxing Yuan, Kyohei Takae, and Hajime Tanaka, Impact of inverse squeezing flow on the self-assembly of oppositely charged colloidal particles under electric field, *Phys. Rev. Lett.* **129**, 248001 (2022).
- [38] Rakwoo Chang and Arun Yethiraj, Solvent effects on the collapse dynamics of polymers, *J. Chem. Phys.* **114**, 7688 (2001).
- [39] Hajime Tanaka and Takeaki Araki, Simulation method of colloidal suspensions with hydrodynamic interactions: Fluid particle dynamics, *Phys. Rev. Lett.* **85**, 1338 (2000).
- [40] Akira Furukawa, Michio Tateno, and Hajime Tanaka, Physical foundation of the fluid particle dynamics method for colloid dynamics simulation, *Soft Matter* **14**, 3738 (2018).
- [41] Kyohei Takae and Hajime Tanaka, Hydrodynamic simulations of charge-regulation effects in colloidal suspensions, *Soft Matter* **14**, 4711 (2018).
- [42] Hans Jörg Limbach and Christian Holm, Single-chain properties of polyelectrolytes in poor solvent, *J. Phys. Chem. B* **107**, 8041 (2003).
- [43] P. P. Ewald, Die Berechnung optischer und elektrostatischer Gitterpotentiale, *Ann. Phys. (Leipzig)* **369**, 253 (1921).
- [44] Daan Frenkel and Berend Smit, *Understanding Molecular Simulation*, 2nd ed. (Academic, San Diego, 2002).
- [45] Francis H. Harlow and J. Eddie Welch, Numerical calculation of time-dependent viscous incompressible flow of fluid with free surface, *Phys. Fluids* **8**, 2182 (1965).
- [46] Zecheng Gan and Zhenli Xu, Multiple-image treatment of induced charges in Monte Carlo simulations of electrolytes near a spherical dielectric interface, *Phys. Rev. E* **84**, 016705 (2011).
- [47] Issei Nakamura and Zhen-Gang Wang, Effects of dielectric inhomogeneity in polyelectrolyte solutions, *Soft Matter* **9**, 5686 (2013).
- [48] Tine Curk, Jiaxing Yuan, and Erik Luijten, Accelerated simulation method for charge regulation effects, *J. Chem. Phys.* **156**, 044122 (2022).
- [49] See Supplemental Material at <http://link.aps.org/supplemental/10.1103/PhysRevLett.132.038101> on the information about simulation details, analysis methods, model limitations, additional characterization, and the movies of polyelectrolyte collapse, which includes Refs. [50,51].
- [50] Ulrich Essmann, Lalith Perera, Max L. Berkowitz, Tom Darden, Hsing Lee, and Lee G. Pedersen, A smooth particle mesh Ewald method, *J. Chem. Phys.* **103**, 8577 (1995).
- [51] Jiuyang Liang, Pan Tan, Yue Zhao, Lei Li, Shi Jin, Liang Hong, and Zhenli Xu, Superscalability of the random batch Ewald method, *J. Chem. Phys.* **156**, 014114 (2022).
- [52] Giacomo Fiorin, Michael L. Klein, and Jérôme Hénin, Using collective variables to drive molecular dynamics simulations, *Mol. Phys.* **111**, 3345 (2013).
- [53] Cameron F Abrams, N-K Lee, and SP Obukhov, Collapse dynamics of a polymer chain: Theory and simulation, *Europhys. Lett.* **59**, 391 (2002).
- [54] M. Smoluchowski, Drei vortrage uber diffusion, brownsche bewegung und koagulation von kolloidteilchen, *Z. Phys.* **17**, 557 (1916), <https://jbc.bj.uj.edu.pl/dlibra/publication/411756/edition/387534/content>.
- [55] Akira Onuki, *Phase Transition Dynamics* (Cambridge University Press, Cambridge, England, 2002).
- [56] Michio Tateno and Hajime Tanaka, Numerical prediction of colloidal phase separation by direct computation of Navier–Stokes equation, *npj Comput. Mater.* **5**, 40 (2019).
- [57] Weronika Szczesna, Justyna Ciejka, Lilianna Szyk-Warszynska, Ewelina Jarek, Kazimiera A. Wilk, and Piotr Warszynski, Customizing polyelectrolytes through hydrophobic grafting, *Adv. Colloid Interface Sci.* **306**, 102721 (2022).
- [58] Luke J. Kirwan, Georg Papastavrou, Michal Borkovec, and Sven H. Behrens, Imaging the coil-to-globule conformational transition of a weak polyelectrolyte by tuning the polyelectrolyte charge density, *Nano Lett.* **4**, 149 (2004).
- [59] I. M. Lifshitz and V. V. Slyozov, The kinetics of precipitation from supersaturated solid solutions, *J. Phys. Chem. Solids* **19**, 35 (1961).



- [60] Carl Wagner, Theory of precipitate change by redissolution, *Z. Elektrochem.* **65**, 581 (1961).
- [61] Roland G Winkler, Michael Gold, and Peter Reineker, Collapse of polyelectrolyte macromolecules by counterion condensation and ion pair formation: A molecular dynamics simulation study, *Phys. Rev. Lett.* **80**, 3731 (1998).
- [62] Meng Li, Aniket Pal, Amirreza Aghakhani, Abdon Pena-Francesch, and Metin Sitti, Soft actuators for real-world applications, *Nat. Rev. Mater.* **7**, 235 (2022).
- [63] JD Honeycutt and D Thirumalai, The nature of folded states of globular proteins, *Biopolymers* **32**, 695 (1992).
- [64] A. Baumketner and Y. Hiwatari, Influence of the hydrodynamic interaction on kinetics and thermodynamics of minimal protein models, *J. Phys. Soc. Jpn.* **71**, 3069 (2002).
- [65] Changbong Hyeon and D. Thirumalai, Capturing the essence of folding and functions of biomolecules using coarse-grained models, *Nat. Commun.* **2**, 487 (2011).